

Deformable Mamba for Wide Field of View Segmentation

Jie Hu^{1,*}, Junwei Zheng^{1,*}, Jiale Wei¹, Jiaming Zhang^{1,2,†}, Rainer Stiefelhagen¹

¹Karlsruhe Institute of Technology, ²ETH Zurich

<https://github.com/JieHu1996/DeformableMamba>

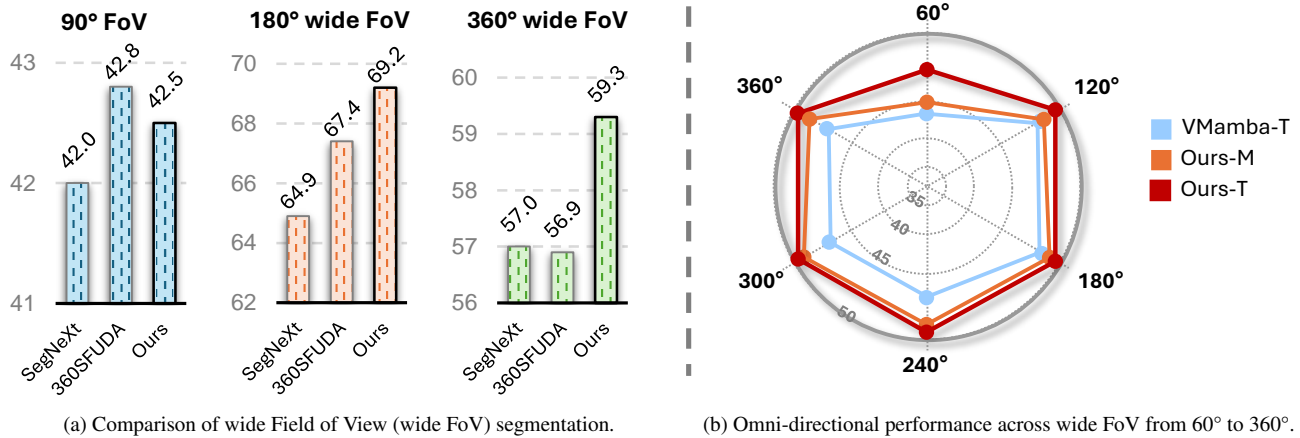


Figure 1. Wide Field of View (wide-FoV) segmentation is investigated on 180° and 360° images. (a) Compared to other methods tailored for 90° or 180° data, our unified Deformable Mamba framework generalizes well on wide-FoV segmentation. (b) Besides, our methods yield consistently better results (mIoU %) across all different FoVs as compared to the baseline on the 360° Matterport3D dataset.

Abstract

Wide-FoV cameras, like fisheye and panoramic setups, are essential for broader perception but introduce significant distortions in 180° and 360° images, complicating dense prediction tasks. For instance, existing MAMBA models lacking distortion-aware capacity cannot perform well in panoramic semantic segmentation. To address this problem, this work presents Deformable Mamba, a unified framework specifically designed to address imaging distortions within the context of panoramic and fisheye semantic segmentation. At the core is a decoder constructed with a series of Deformable Mamba Fusion (DMF) blocks, making the whole framework more deformable, efficient, and accurate, when handling extreme distortions. Extensive evaluations across five datasets demonstrate that our method consistently improves segmentation accuracy compared to the previous state-of-the-art methods tailored for specific FoVs. Notably, Deformable Mamba achieves a +2.5% performance improvement on the 360° Stanford2D3D dataset,

and shows better results across FoVs from 60° to 360°.

1. Introduction

Dense image analysis like image segmentation [2, 21, 58] is a fundamental task in computer vision, forming a crucial component of numerous downstream vision-based applications [70]. At the same time, advancements in sensor technology have led to a variety of sensor types, each with unique characteristics that impact imaging. In recent years, diverse sensors such as pinhole cameras, fisheye cameras [48, 64] with 180° field of views (FoV), and even panoramic cameras [1, 3, 67] with 360° FoV have been increasingly adopted across vision tasks. However, differences in camera construction and sensor type result in distinct imaging characteristics, which can complicate traditional image processing [66]. Adapting algorithms to perform effectively with a specific FoV often requires considerable time and resources, involving method redesign, parameter tuning, and model retraining to address the unique challenges posed by each camera type.

Based on our experiments (Fig. 1a), we observe that

*Equal contribution.

†Corresponding author (e-mail: jiaming.zhang@kit.edu).

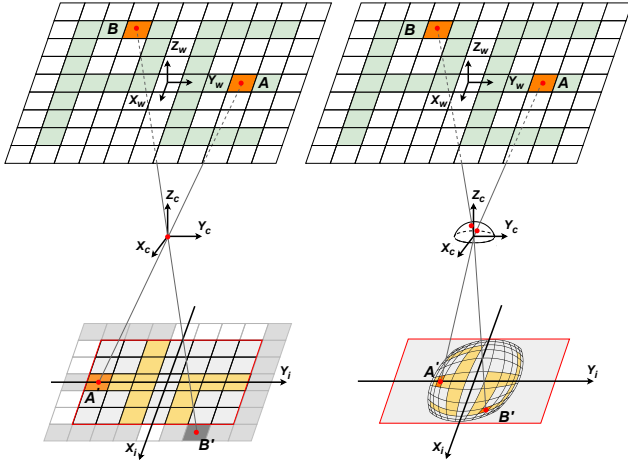


Figure 2. Comparison of camera imaging with pinhole (left) and fisheye (right) cameras with different wide-FoV. Pinhole cameras maintain geometric fidelity but limited coverage, whereas wide-FoV cameras offer expansive scene capture while introducing substantial geometric distortions.

straightforwardly applying or transferring existing specific models to new sensor types frequently leads to significant performance degradation. For instance, methods [21] specifically designed for narrow-FoV pinhole cameras typically cannot generalize well when used for analyzing fisheye images with 180° FoV. This is primarily due to the high degree of image distortion and object deformation present in wide-FoV cameras, which complicates model generalization. Standard methods struggle to accurately capture the diverse object shapes and spatial distributions caused by such deformations. For instance, as shown in Fig. 2, the altered pixel arrangement in wide-FoV images might lead to misclassifications and limits their adaptability. Previous methods have proposed solutions targeting specific sensor types, such as CNN-based and transformer-based semantic segmentation models [31, 52] optimized for fisheye images, as well as approaches [66, 67] tailored to mitigate distortion in panoramic segmentation. So far, to address diverse distortions across different camera types in a unified manner remains under-explored.

To address these challenges, we propose the **Deformable Mamba** model (DMamba for short), a versatile solution for image segmentation across varying wide-FoVs. In this work, a unified framework is created to effectively handling images from multiple camera types and sources, spanning FoVs from 180° to 360° , from indoor to outdoor scenarios, in synthetic and real-world imageries. At the core of our approach is a novel **deformable decoder**, which synergistically integrates State Space Models (SSMs) with deformable convolutions. Specifically, we leverage quadri-directional selective scan operations derived from VMamba [37] to capture global contextual information, while simultaneously employing deformable con-

volution [77] to enhance feature representation. This dual-pathway design effectively addresses the limitations of scanning mechanisms of Mamba [16] in visual applications while also endowing the model with the ability to perceive distortion. Our deformable decoder accommodates varied receptive fields, enabling seamless integration with CNN-based, transformer-based, and Mamba-based architectures. By leveraging this unified decoder, Deformable Mamba effectively captures features across disparate imaging perspectives, making it an adaptable solution for segmentation tasks across a broad spectrum of camera types.

To evaluate the effectiveness of Deformable Mamba, we conducted extensive experiments across five datasets for semantic segmentation, including three 360° (SynPASS [67], Stanford2D3D [1], Matterport3D [3]) and two 180° (WoodScape [64], SynWoodScape [48]) datasets. The data encompass a variety of scenarios including 180° and 360° images, indoor and outdoor environments, and both synthetic and real-world data. Our unified framework performs consistently well across various datasets. Notably, on 360° Stanford2D3D dataset, Deformable Mamba achieved state-of-the-art performance, with a $+2.5\%$ absolute improvement over the pinhole Mamba model. In 180° SynWoodScape dataset, it similarly surpassed prior best-performing models, achieving an increase of $+2.2\%$ in mean Intersection over Union (mIoU). Further ablation studies, including comprehensive omni-directional comparisons, consistently demonstrated the model’s effectiveness in handling wide-FoVs, showing its potential as a general solution for dense image analysis across diverse sensor types. We hope this work opens up new possibilities for unifying wide-FoV segmentation.

To summarize, our contributions are as follows.

- We propose a Mamba-based framework termed Deformable Mamba, with the aim at unifying distortion-aware wide-FoV segmentation.
- A deformable decoder constructed with Deformable Mamba Fusion (DMF) module is specifically designed to boost the performance of mamba-based models in the wide-FoV segmentation task.
- Extensive experiments on five datasets across a variety of indoor and outdoor, synthetic and real-world wide-FoV scenes, demonstrate the state-of-the-art performance of our method in wide-FoV segmentation.

2. Related Work

2.1. Wide Field of View Segmentation

Wide Field-of-View (Wide-FoV) semantic segmentation has received increasing attention as it enables broader scene understanding in applications such as autonomous driving and robotics. However, directly applying pinhole models [2, 5, 6, 9, 15, 19, 26, 34, 36, 39, 50, 58, 65, 65, 70, 72]

to wide-FoV images often results in downgraded performance due to object deformations and image distortions. Previous work [61, 62] propose the Panoramic Annular Semantic Segmentation (PASS) framework using a panoramic annular lens system. [27] introduces panoramic panoptic segmentation for panoramic views. In [66, 67], deformable modules are proposed to enhance the distortion perception capability in transformers. Zheng *et al.* [71] introduce the Open Panoramic Segmentation (OPS) task in an open-vocabulary context. Apart from panoramas, previous methods [11, 31] revolve around multi-task on fisheye images, while a pretraining paradigm [42] and semi-supervised approaches [43, 45] are introduced to address the challenges of fisheye data. Manzoor *et al.* [40] substitutes the conventional convolutional modules in U-Net [47] and residual U-Net [46] with restricted deformable convolution (RDC) [11], imparting fisheye-distortion awareness to the model. Departing from these approaches, we are the first to propose a unified model applicable to all wide-FoV inputs, including panoramic and fisheye images.

2.2. State Space Model

CNNs [30] have achieved remarkable success in computer vision through effective local feature extraction and hierarchical representation learning capabilities, while Transformers [54] excel at modeling long-range dependencies despite their quadratic computational complexity. Recently, the state-space-model (SSM) based Mamba [16] architecture has emerged as a promising alternative, offering linear complexity and parallel computation through its selective scan mechanism, ushering in a new paradigm for long sequence modeling. The emergence of Mamba in sequence modeling has naturally extended to vision tasks, Zhu *et al.* [75] adopt the patch embedding from Vision Transformer (ViT) [12] to project 2D image patches into sequential tokens compatible with Mamba architecture. To address the inherent discrepancy between image and sequence representations, a quadri-directional scanning and merging mechanism termed SS2D is introduced in [37] to supersede Mamba’s canonical 1D scan operation. Subsequent work [4, 24, 25, 32, 44, 63, 69] introduce various scanning methods to explore variations of Mamba in visual representations. However, the study of using SSM for wide-FoV imagery is under-explored. Therefore, for the first time, we propose deformable Mamba to address both panoramic and fisheye semantic segmentation.

3. Methodology

3.1. Preliminary

Image Distortion. As shown in the left side of Fig. 2, the point A in the world coordinates undergoes extrinsic transformation to camera coordinates by Eq. (1), where R and

T denote the rotation matrix and translation vector, respectively. Following Eq. (2), points in the camera coordinates are projected onto the image plane, with f_x and f_y representing the focal lengths and c_x, c_y defining the principal point. While straight lines are preserved in pinhole-approximate narrow-FoV cameras, only points within the sensor’s FoV (red box in Fig. 2) are imaged, excluding points like B' that fall outside this region. Narrow-FoV cameras follow perspective projection principles where object size in the image varies inversely with distance between object and camera, introducing moderate distortion.

$$\begin{bmatrix} \mathbf{X}_c \\ \mathbf{Y}_c \\ \mathbf{Z}_c \end{bmatrix} = \mathbf{R} \begin{bmatrix} \mathbf{X}_w \\ \mathbf{Y}_w \\ \mathbf{Z}_w \end{bmatrix} + \mathbf{T}, \quad (1)$$

$$\begin{bmatrix} x' \\ y' \\ 1 \end{bmatrix} = \begin{bmatrix} f_x & 0 & c_x \\ 0 & f_y & c_y \\ 0 & 0 & 1 \end{bmatrix} \begin{bmatrix} \frac{\mathbf{X}_c}{\mathbf{Z}_c} \\ \frac{\mathbf{Y}_c}{\mathbf{Z}_c} \\ 1 \end{bmatrix}. \quad (2)$$

In contrast, wide-FoV cameras like fisheye cameras employ complex projection models involving light refraction. Kannala *et al.* [28] propose a generalized projection model for wide-FoV cameras, the distance between the image point and the principal point r is approximated by:

$$r(\theta) = \mathbf{k}_1\theta + \mathbf{k}_2\theta^3 + \mathbf{k}_3\theta^5 + \mathbf{k}_4\theta^7 + \mathbf{k}_5\theta^9, \quad (3)$$

where θ is the angle between the principal axis and the incoming ray, $k_i, i \in \{1, 2, 3, 4, 5\}$ are the parameters of wide-FoV camera model. While these cameras capture wider FoV, they suffer from more severe geometric distortions compared to the perspective projection of narrow-FoV cameras. As shown in the right side of Fig. 2, barrel distortion in wide-FoV cameras causes straight lines to appear curved outward, particularly pronounced near image edges while the center remains relatively undistorted. This distortion manifests as radially-increasing displacement from the center, resulting in progressive spatial compression toward the image periphery.

State Space Model. State space model (SSM), which describes the dynamics of a system, can be formulated as:

$$\begin{aligned} \mathbf{h}'(\mathbf{t}) &= \mathbf{A}\mathbf{h}(\mathbf{t}) + \mathbf{B}\mathbf{x}(\mathbf{t}), \\ \mathbf{y}(\mathbf{t}) &= \mathbf{C}\mathbf{h}(\mathbf{t}), \end{aligned} \quad (4)$$

where $x(t)$ and $y(t)$ denote the inputs and outputs of the system, respectively, $h(t)$ is the inner states of the system, A, B, C are the system parameters. Gu *et al.* [18] propose Structured State Space Sequence Model (S4) by initializing the parameters A using Hippo Matrix (5) and discretizing parameters A and B by step size Δ .

$$\mathbf{A}_{nk} = - \begin{cases} (2\mathbf{n} + 1)^{1/2}(2\mathbf{k} + 1)^{1/2} & \text{if } \mathbf{n} > \mathbf{k} \\ \mathbf{n} + 1, & \text{if } \mathbf{n} = \mathbf{k} \\ 0, & \text{if } \mathbf{n} < \mathbf{k}. \end{cases} \quad (5)$$

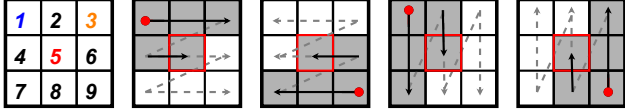


Figure 3. Visualization of SS2D quadri-directional scanning.

In Mamba [16], a selective scan mechanism is proposed to further extend the SSM from time-invariant to time-variant, while also enabling parallel training. **Observations.** Based on HiPPO theory [17], Mamba [16] is inherently a sequence model, where the output of the current token only depends on preceding tokens, without considering subsequent ones - a limitation that becomes problematic for 2D images with inherent spatial structures. Unlike Transformer’s [54] mechanism in ViT [12], where attention computation for each patch considers all patches globally, Mamba processes image patches sequentially.

To address this limitation, previous work [4, 37, 63, 75, 76] have explored different scanning patterns, including bidirectional or quadri-directional scanning approaches, partially addressing the challenges posed by Mamba’s unidirectional scanning nature in visual tasks. However, these multi-directional scanning approaches face another challenge. As illustrated in Fig 3., consider an input image embedded into 9 patches (labeled 1-9). When modeling patch 5 using SS2D’s [37] quadri-directional scanning mechanism, the scanning sequences are:

- (1) Left-Right: 1 - 2 - 3 - 4 - 5
- (2) Right-Left: 9 - 8 - 7 - 6 - 5
- (3) Top-Down: 1 - 4 - 7 - 2 - 5
- (4) Down-Top: 9 - 6 - 3 - 8 - 5

Patch 1 and patch 3 maintain equal distances from patch 5, demonstrating uniform spatial distribution. As illustrated in sequences (1) (3) (4), the scanning trajectory from patch 1 to patch 5 traverses double the path length compared to the direct route between patch 3 and patch 5, despite their equivalent spatial distances. Since the Mamba model learns relationships between serialized tokens, the contribution of earlier patches in the scanning path to the current patch decreases as their distance from the current patch increases. Thus, along this scanning path, we infer that patch 1 is more important to patch 5 than patch 3. This priority is introduced by the scanning mechanism, but it is not a reasonable assumption. Additionally, when computing for other target patches, this priority changes based on the target’s position.

3.2. Overall Architecture

An overview of our Deformable Mamba architecture is presented in Fig. 4, which illustrates how we make Mamba-

based models deformable and available for wide-FoV semantic segmentation. It mainly follows the Encoder-Decoder architecture. The backbone selection is flexible for different methods like CNN-, transformer- or Mamba-based architectures. In this work, we explore with VMamba [37] as the backbone and our proposed Deformable Mamba Decoder. In our framework, there are two model sizes: DMamba-M (Mini) and DMamba-T (Tiny).

More specifically, given the wide-FoV input image in the shape of $H \times W \times 3$, a stem module is firstly utilized to patchify the original image into the shape of $\frac{H}{4} \times \frac{W}{4} \times 3$, the encoder gradually down-samples feature maps in the l^{th} stage with channel dimensions $C_l \in \{96, 192, 384, 768\}$ and resolutions $\in \{\frac{H}{4} \times \frac{W}{4}, \frac{H}{8} \times \frac{W}{8}, \frac{H}{16} \times \frac{W}{16}, \frac{H}{32} \times \frac{W}{32}\}$. The features extracted by the encoder undergo a hierarchical fusion process in the decoder.

3.3. Deformable Mamba Decoder

The Deformable Mamba Decoder comprises four fusion and upsampling modules, where we introduce a novel **Deformable Mamba Fusion (DMF)** module for multi-scale feature integration. The initial DMF block processes dual inputs of $\frac{H}{32} \times \frac{H}{32} \times 768$ feature maps derived from the final encoder layer. The fused features are then processed through an upsampling module that simultaneously reduces channel dimensionality and increases spatial resolution, followed by channel mixing via an MLP layer. Following [35, 49, 60, 68], we utilize Pixel Shuffle [49] as the upsampling operation. In the subsequent stages, the second through fourth DMF blocks implement skip connections, facilitating interaction between the previously fused and upsampled features and their corresponding encoder features at matching scales. This progressive fusion strategy enables comprehensive multi-scale feature integration. The decoder’s output undergoes final processing through a fully connected layer and class mapping to generate the segmentation predictions.

3.4. Deformable Mamba Fusion

To address the aforementioned limitations of Mamba’s scanning mechanism in visual tasks (Sec. 3.1), we propose the DMF module, which simultaneously adapts the features extracted by the Mamba-based encoder and integrates multi-scale features. As illustrated in the lower part of Fig. 4, the DMF module takes two inputs: one is the feature D_j with dimensions $c \times h \times w$ output from the upper decoder layer, and the other is the corresponding encoder features E_i at matching scales, where i and j satisfy the relationship $i + j = 5$. We employ the Cross-Scan [37] that scans D_j in four directions: (1) Left to Right, (2) Right to Left, (3) Top to Down, and (4) Down to Top, utilizing Mamba model’s global perception to generate four feature maps with resolution $c \times h \times w$. Following Cross-Merge [37], we first

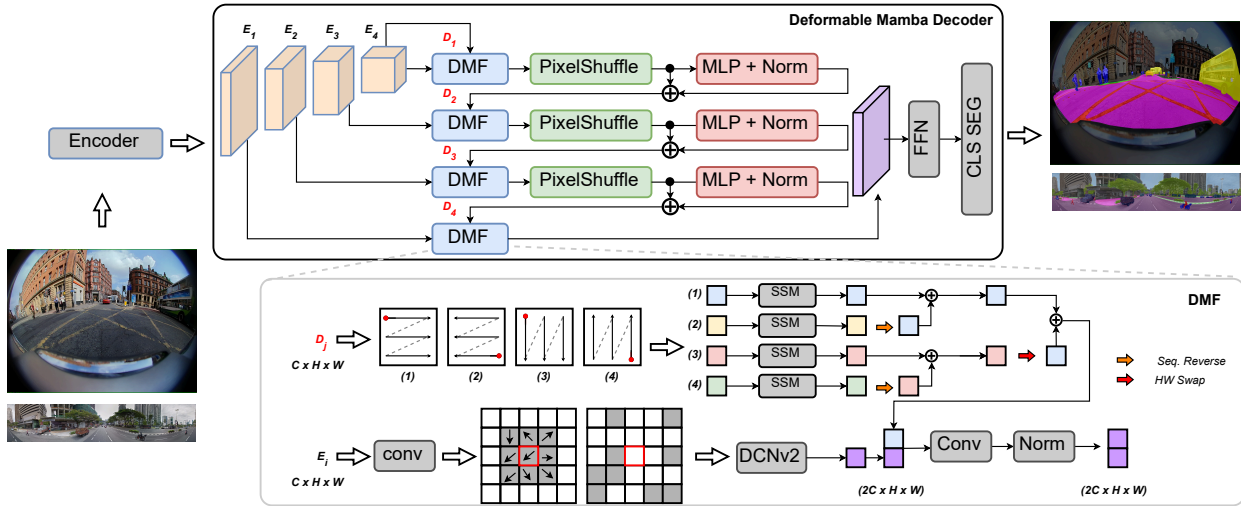


Figure 4. Overview of the Deformable Mamba (DMamba) framework. Given wide-FoV images (180° or 360°), the features extracted by an encoder, are fused by the proposed Deformable Mamba Decoder, which constructed by four Deformable Mamba Fusion (DMF) modules.

reverse features (2) and (4) along their last dimension and add them to (1) and (3) respectively, then transpose the h and w dimensions of feature (3) before adding it to (1).

Inspired by previous works [10, 56, 59, 77], we propose a simple yet effective approach, utilizing deformable convolution [77] to enhance the features extracted by the Mamba model. Specifically, for a feature point in the encoder feature map E_i , we attend to K neighboring feature points, allowing the model to learn offsets that compensate for the biases introduced by the scanning process. Additionally, convolution operations on these selected regions provide a more localized attention mechanism, further enhancing the visual representation capability of Mamba-based models in visual tasks. The mathematical formulation is as follows:

$$y(\mathbf{p}) = \sum_{k=1}^K \mathbf{w}_k \mathbf{m}_k \mathbf{x}(\mathbf{p} + \mathbf{p}_k + \Delta \mathbf{p}_k), \quad (6)$$

where \mathbf{p} denotes the current location in feature map, \mathbf{w}_k and \mathbf{p}_k denote the weight and initial offsets for the k -th location, respectively. And \mathbf{m}_k is a learnable modulation scalar, which helps to modulate the input feature amplitudes from different spatial locations. For example, $K = 9$ and $\mathbf{p}_k \in (-1, -1), \dots, (1, 1)$ defines a 3×3 convolutional kernel with dilation 1.

The outputs from these two branches are concatenated and fed into a convolutional layer for feature fusion. This simple yet effective architecture successfully adapts the features extracted by the Mamba model, efficiently integrates multi-scale features, while endowing the entire decoder with deformable capabilities. Experiments on multiple datasets demonstrate both the effectiveness and efficiency of our proposed model.

4. Experiment Results

4.1. Datasets

To study the unification of wide-FoV segmentation, we conduct experiments on three 360° and two 180° datasets.

Stanford2D3D [1] consists of 1,413 indoor 360° images with a resolution of 512×1024 , encompassing 13 distinct object categories.

Matterport3D [3] has 10,615 indoor 360° images. Following [22, 53], 7,829 of panoramas with a resolution of 1024×2048 are used for training and 772 for evaluation.

SynPASS [67] is a virtual outdoor 360° dataset from CARLA [13]. It contains 9,080 images with a resolution of 1024×2048 , covering various weather conditions (cloudy, foggy, rainy, sunny) and illumination (daytime, nighttime).

WoodScape [64] consists of 10K 180° images captured by four surround view cameras. The semantic labels have 9 categories. Since the test split is not available, 8,234 released images are reallocated into training and evaluation sets with an 80% to 20% split.

SynWoodScape [48] is a synthetic version of the surround-view dataset. The released v0.1.1 version contains 2,000 180° surround-view fisheye RGB images. We split them into training and validation sets with an 80% to 20% ratio.

4.2. Implementation Details

In this work, our models are trained and validated on three 360° datasets and two 180° datasets, covering both indoor and outdoor scenarios, as well as real and synthetic environments, using 4 A100 GPUs. For all experiments, we employed cross-entropy as the loss function. To validate the effectiveness of our framework, we deliberately avoided

Table 1. **Results on 360° segmentation datasets** of Stanford2D3D (S2D3D) fold-1 and 360FV-Matterport (MP3D). †denotes our re-implementation.

Method	Backbone	mIoU	
		S2D3D	MP3D
Tangent [14] (CVPR20)	ResNet-101	45.6	-
HoHoNet [51] (CVPR21)	ResNet-101	52.0	44.1
CBFC [74] (CVPR23)	ResNet-101	52.2	-
Trans4PASS [66] (CVPR22)	Trans4PASS	52.1	41.9
Trans4PASS+ [67] (PAMI24)	Trans4PASS+	54.0	42.6
SegFormer-B2† [58] (NeurIPS21)	MiT-B2	51.9	45.5
360BEV [53] (WACV24)	MiT-B2	54.3	46.3
SGAT4PASS [33] (IJCAI23)	MiT-B2	56.4	-
360SFUDA† [73] (CVPR24)	MixT-B2	54.9	46.7
360SFUDA† [73] (CVPR24)	MixT-B3	56.9	47.9
SegNeXt† [21] (NeurIPS22)	MSCAN-B	57.0	48.4
VMamba† [37] (NeurIPS24)	VMamba-T	56.8	47.6
DMamba-M (Ours)	VMamba-T	59.3	48.7
DMamba-T (Ours)	VMamba-S	60.2	49.3

using any auxiliary losses. The models were optimized using AdamW with an initial learning rate of $6e^{-5}$ and weight decay of 0.01. For Stanford2D3D and SynWoodScape, we trained for 80K iterations with a batch size of 2 per GPU. For Matterport3D, SynPASS, and WoodScape, we extended the training to 160K iterations, maintaining the same batch size of 2 per GPU. The learning rate schedule consisted of a linear warm-up for the first 1.5K iterations, followed by a polynomial decay with a power of 0.9.

4.3. Quantitative Results

Given that previous works were largely constrained to specific Field-of-View (FoV) settings, which poses challenges for fair cross-dataset evaluation. Therefore, we selected representative state-of-the-art models as our baselines, including SegNeXt [21], which achieves superior performance on pinhole images, and 360SFUDA [73], which is specifically designed for panoramic scenarios. To ensure fair comparison, we carefully match the parameter counts across all implementations and conduct extensive evaluations on the aforementioned datasets with varying FoV characteristics.

Results on 360° Stanford2D3D. Table 1 shows superior performance of our method compared to both panoramic [14, 33, 51, 53, 66, 67, 73, 74] and pinhole-based [21, 37] methods. Specifically, our model with the VMamba-T as backbone achieves a significant mIoU improvement of +2.9% to +13.7% over panoramic baselines.

Notably, compared to the VMamba-T + UperNet [57], our lightweighted DMamba-M with the same backbone achieves a +2.5% higher mIoU while reducing parameter count by 30% and FLOPs by 80%. Furthermore, our DMamba-T model, which has a comparable parameter count to VMamba-T + UperNet, demonstrates even better performance with a +3.4% mIoU improvement.

Results on 360° Matterport3D.

While our DMamba-M demonstrates remarkable performance on Stanford2D3D dataset, the challenge becomes more pronounced on large-scale Matterport3D panoramic datasets, where we observe a relatively modest improvement margin of 0.3 mIoU over the previous SOTA model SegNeXt as shown in Table 1. Remarkably, our DMamba-T achieves more substantial gains of +0.9% and +1.7% mIoU compared to SegNeXt and VMamba-T respectively, with comparable model capacities.

Results on 360° SynPASS. Beyond real-world datasets, we evaluate the generalizability of our method on synthetic and outdoor scenes on the SynPASS dataset. It is worth noting that despite SegNeXt’s superior performance over 360SFUDA in real-world scenarios, it exhibits a substantial performance degradation on the synthetic dataset. This discrepancy underscores the sensitivity of certain architectures to distribution shifts. In contrast, our method, as shown in Table 2, achieves the state-of-the-art mIoU of 42.78%, surpassing all existing panoramic- and pinhole-based methods. Specifically, our DMamba-T overall achieves top scores on *pedestrian*, *pole*, *traffic sign*, *static* and *dynamic*. For *traffic sign* with slender properties, our model enjoys more than +6.0% mIoU.

Results on 180° WoodScape. In Table 3, we present a comparison of our method with other models using 180° fisheye inputs from the WoodScape dataset [64]. Semi-supervised methods such as MeanTeacher [52], CPS [7], and FishSegSSL [43] show lower performance due to the limited data. Compared to multi-task models, our proposed DMamba, designed with deformable settings, outperforms all variants of the OmniDet [31] model.

Although SegNeXt and 360SFUDA perform well on the WoodScape dataset, our method, with a more compact architecture still achieves a higher mIoU by +0.9% and +0.8%, respectively. The DMamba-T variant further advances the state-of-the-art mIoU to 83.9%, confirming DMamba’s effectiveness in capturing heavily distorted object information in wide-FoV segmentation.

Results on 180° SynWoodScape. Due to the lack of baseline comparisons on SynWoodScape, we limited our evaluation to SegNeXt and 360SFUDA. Similar to the results on SynPASS, SegNeXt and 360SFUDA perform similarly on real 180° datasets, while the former exhibits a significant performance degradation on synthetic 180° data. This further confirms the challenge of achieving consistently high performance across diverse datasets. In comparison, our DMamba-M of similar scale outperforms them by +4.36% and +1.73% mIoU, respectively, achieving an improved segmentation accuracy of 69.20 mIoU on SynWoodScape.

These consistent improvements across all five wide-FoV datasets demonstrate the effectiveness of our proposed framework in unifying wide-FoV segmentation.

Table 2. **Results on 360° segmentation dataset** SynPASS. †denotes our re-implementation.

Method	mIoU	Building	Fence	Other	Pedestrian	Pole	RoadLine	Road	SideWalk	Vegetation	Vehicles	Wall	TrafficSign	Sky	Ground	Bridge	RailTrack	GroundRail	TrafficLight	Static	Dynamic	Water	Terrain
PVT-T [55] (CVM22)	32.37	74.83	19.94	00.24	21.82	13.15	62.59	93.14	49.09	67.27	46.44	01.69	09.63	96.09	00.18	02.64	08.81	61.11	14.09	12.04	00.99	05.05	51.33
PVT-S [55] (CVM22)	32.68	78.02	27.12	00.27	23.48	16.51	59.81	92.87	50.21	66.22	43.50	01.12	08.67	96.34	00.44	00.15	02.82	63.88	13.78	15.15	01.58	08.78	48.29
SegFormer-B1 [58] (NeurIPS21)	37.36	78.24	20.59	00.00	38.28	21.09	68.72	94.50	59.72	68.43	67.51	00.83	09.86	96.08	00.56	01.38	20.79	69.59	23.38	19.91	01.38	08.97	52.07
SegFormer-B2 [58] (NeurIPS21)	37.24	79.25	23.58	00.00	40.01	20.14	65.28	92.80	46.92	68.64	77.45	01.42	15.00	96.33	00.57	00.58	02.68	67.60	25.89	20.80	01.99	20.92	51.53
Trans4PASS-T [66] (CVPR22)	38.53	79.17	28.18	00.13	36.04	23.69	69.16	95.51	61.71	69.77	71.12	01.53	16.98	96.50	00.56	01.60	15.22	70.48	26.03	23.11	02.08	09.24	49.77
Trans4PASS-S [66] (CVPR22)	38.57	80.02	24.56	00.07	41.49	25.23	72.00	95.89	59.88	69.07	77.08	01.04	13.72	96.69	00.67	00.73	05.60	72.56	25.93	22.45	02.78	08.34	52.65
Trans4PASS+(T) [67] (PAMI24)	39.42	79.63	24.45	00.21	44.23	26.71	70.32	95.86	61.80	69.25	78.85	01.09	13.81	97.12	00.91	03.48	19.32	72.44	21.08	25.56	02.67	05.03	53.20
Trans4PASS+(S) [67] (PAMI24)	40.72	80.91	20.78	00.23	45.36	24.08	72.51	96.79	67.15	70.46	81.39	04.28	26.19	97.21	01.24	01.74	16.56	67.08	28.64	23.68	03.35	08.48	57.57
SegNeXt-B† [21] (NeurIPS22)	39.90	82.62	16.06	00.12	43.21	26.15	71.69	97.10	60.64	67.56	82.56	00.32	24.43	97.23	02.03	00.00	43.23	47.90	31.61	26.50	03.63	10.56	42.68
360SFUDA-B2† [73] (CVPR24)	40.37	82.69	22.27	00.16	41.86	28.19	74.98	97.13	62.22	70.05	81.55	04.21	21.09	97.45	01.06	00.49	31.77	51.08	32.15	24.88	03.59	10.02	49.23
360SFUDA-B3† [73] (CVPR24)	41.33	82.91	32.33	00.23	41.87	27.21	75.13	97.37	62.90	69.34	82.95	01.66	26.03	97.56	00.95	00.10	41.39	64.02	32.30	26.74	03.48	16.76	48.14
DMamba-M(Ours)	41.72	83.19	21.52	00.21	48.15	32.20	75.8	97.51	61.00	67.74	81.86	01.06	31.30	94.47	01.37	00.68	29.63	49.41	36.35	30.99	04.08	20.54	45.27
DMamba-T(Ours)	42.78	84.24	22.57	00.25	49.20	33.25	76.85	98.56	62.05	68.79	82.91	02.11	32.35	98.52	02.42	01.73	30.68	50.46	37.40	32.04	05.85	21.59	46.32

Table 3. **Results on 180° segmentation dataset** WoodScape. †denotes our re-implementation.

Method	Multitask	Supervised	mIoU
MeanTeacher [52] (NeurIPS17)	✗	✗	54.20
CPS [7] (CVPR21)	✗	✗	60.31
CPS with CutMix [7] (CVPR21)	✗	✗	62.47
FishSegSSL [43] (J. Imaging24)	✗	✗	64.81
OmniDet [31] (RA-L21)	✗	✓	72.50
+ DTP [20] (ECCV18)	✓	✓	75.80
+ GradNorm [8] (PMLR18)	✓	✓	75.90
+ Uncertainty [29] (CVPR18)	✓	✓	76.10
+ VarNorm [31] (RA-L21)	✓	✓	76.60
SegNeXt-B† [21] (NeurIPS22)	✗	✓	82.32
360SFUDA-B2† [73] (CVPR24)	✗	✓	81.74
360SFUDA-B3† [73] (CVPR24)	✗	✓	82.43
DMamba-M (Ours)	✗	✓	83.21
DMamba-T (Ours)	✗	✓	83.90

Table 4. **Results on 180° segmentation dataset** SynWoodScape. †denotes our re-implementation.

Method	mIoU
SegNeXt-B† [21] (NeurIPS22)	64.86
360SFUDA-B2† [73] (CVPR24)	66.56
360SFUDA-B3† [73] (CVPR24)	67.47
DMamba-M (Ours)	69.20
DMamba-T (Ours)	69.62

4.4. Qualitative Results

To demonstrate the improved performance of our model over Mamba-based models, we compared the visualization results of DMamba and VMamba on the Stanford2D3D and SynWoodScape. As discussed in Sec. 3.1 and 3.4, the scanning approach in Mamba-based models introduces biases in visual tasks that limit their effectiveness in dense prediction tasks. These biases increase randomness and reduce the model’s ability to capture local spatial relationships, which is particularly evident in the recognition and segmentation of smaller objects. As shown in Fig. 5, the baseline model struggles to accurately segment narrow and elongated areas such as door frames, vegetation contours, traffic light poles,

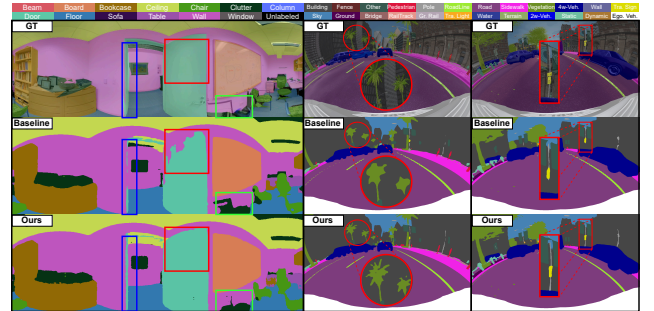


Figure 5. Visualization of the wide-FoV segmentation results. From left to right: one 360° and two 180° segmentation.

and lane markings. In contrast, our proposed DMamba effectively addresses these challenges, significantly improving segmentation performance on small and elongated objects.

4.5. Ablation Study

Effect of Backbone. In Table 5, we ablate three different kinds of commonly-used model backbones, namely CNN-based ResNet [23], ViT-based Swin Transformer [38] and Mamba-based VMamba [37]. For the sake of a fair comparison, we choose the backbones with a comparable number of learnable parameters and FLOPs. According to Table 5 it can be observed that the models equipped with VMamba [37] outperform other models consistently while CNN-based ResNet50 and ViT-based Swin Transformer achieve similar performance. This conclusion can be validated by employing the same decoder, such as Uper-Head [57], MusterHead [60], CGRHead [41], and our proposed DMambaHead, along with a consistent model backbone to perform the segmentation task. Notably, the combination of the VMamba [37] backbone with DMambaHead, resulting in our Deformable Mamba model, demonstrates superior performance compared to other variant combina-

Table 5. **Ablation study** for analysis of backbones (BB) and decoders (Dec) on the 360° dataset Stanford2D3D.

Method	Backbone (BB)	Decoder (Dec)	FPS	Params (M) ↓			FLOPs (G) ↓			Results ↑	
				BB	Dec	Total	BB	Dec	Total	mIoU	mAcc
ResNet-UperNet	ResNet50 [23]	UperHead [57]	44.3	23.5	40.5	64.0	22.9	250.7	273.6	53.34	62.42
ResNet-UperFormer	ResNet50 [23]	MusterHead [60]	14.3	23.5	203.1	226.6	22.9	211.5	234.4	54.39	63.27
ResNet-CGRSeg	ResNet50 [23]	CGRHead [41]	58.0	23.5	282.6	306.1	22.9	31.4	54.3	54.12	62.94
ResNet-DMamba (Ours)	ResNet50 [23]	DMambaHead	27.9	23.5	77.3	100.8	22.9	38.8	61.7	57.22	66.32
Swin-UperNet	Swin-T [38]	UperHead [57]	34.9	27.5	31.5	59.0	25.6	211.5	237.1	53.82	63.06
Swin-UperFormer	Swin-T [38]	MusterHead [60]	30.2	27.5	19.1	46.6	25.6	21.9	47.5	52.36	54.54
Swin-CGRSeg	Swin-T [38]	CGRHead [41]	52.2	27.5	40.6	68.1	25.6	5.5	31.1	54.26	62.90
Swin-DMamba (Ours)	Swin-T [38]	DMambaHead	37.3	27.5	11.2	38.7	25.6	6.5	32.1	55.09	65.30
VMamba-UperNet	VMamba-T [37]	UperHead [57]	35.0	29.5	31.5	61.0	25.3	206.9	232.2	56.80	65.01
VMamba-UperFormer	VMamba-T [37]	MusterHead [60]	29.8	29.5	19.1	48.6	25.3	21.4	46.7	58.12	66.97
VMamba-CGRSeg	VMamba-T [37]	CGRHead [41]	42.2	29.5	40.5	70.0	25.3	5.0	30.3	56.45	65.07
DMamba-M (Ours)	VMamba-T [37]	DMambaHead	40.0	29.5	11.1	40.6	25.3	6.0	31.3	59.30	68.99
DMamba-T (Ours)	VMamba-S [37]	DMambaHead	17.9	49.4	11.1	60.5	44.7	6.0	50.7	60.18	71.68

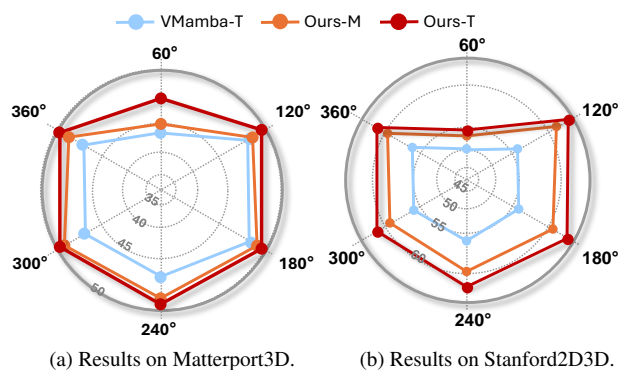


Figure 6. Analysis of segmentation with different wide FoVs.

tions by a maximum of over +6.9% mIoU.

Effect of Decoder. Apart from the backbones, we also ablate the decoders. For every backbone, we conduct four experiments with different decoders, *i.e.*, UperHead [57], MusterHead [60], CGRHead [41], and our proposed DMambaHead. All results are reported in Table 5. Using the same model backbone, our proposed DMambaHead outperforms other widely-used decoders by a +3% mIoU while a complexity degradation of +20%, making the Deformable Mamba and its variants extremely practical in real-time wide-FoV accurate segmentation. It’s worth noting that the DMambaHead with VMamba-T [37] backbone achieves a drop of FLOPs from 232.2G to 31.3G, a drop of the learnable parameters from 61M to 40.6M while the performance of Deformable Mamba increases from a +56.8% to +59.3% mIoU compared with the VMamba-T [37] and UperHead [57] combination. The reason behind this is that our proposed DMambaHead is specifically designed for wide-FoV segmentation. Our deformable design enables the model to focus on the distortion introduced by the wide-FoV fisheye or panoramic images. This ablation proves that not only the VMamba [37] backbone but also the proposed DMambaHead contributes to the superior performance and efficiency of the Deformable Mamba model.

Analysis of FoVs. To further analyze the wide-FoV segmentation, we conduct omni-directional analysis. As shown in Fig. 6, there are six different FoVs, ranging from 60° to 360°. Compared to the baseline VMamba [37], our DMamba methods obtain relative better results on all different FoVs. Note that the 60° performance of all methods are lower than other degrees on the Stanford2D3D dataset. One reason is that the object distribution and room layout in the 60° direction are different between Stanford2D3D and the Matterport3D datasets. Nonetheless, our Mini- and Tiny-version methods show consistent improvements over the baseline on both datasets in different FoVs.

5. Conclusion

In this work, we are the first to explore the unification of the wide field of view (FoV) segmentation tasks, including 180° and 360° image segmentation. Most existing models are tailored for pinhole camera images, making it challenging to extend their success to wide-FoV domains due to the severe image distortion and object deformation. Unlike previous approaches that require a specific architecture for each FoV or dataset, we propose a unified framework, Deformable Mamba, built on the emerging State Space Model (SSM) mechanism. Our framework is constructed with a flexible deformable decoder, which can be easily adapted to various models and datasets. Consistent improvements across five diverse wide-FoV datasets, ranging from indoor to outdoor, from synthetic to real-world scenes, demonstrate that our unified framework effectively addresses the unique challenges of wide-FoV segmentation.

Limitations and Future Work. Using large language models (LLMs) for unifying the wide-FoV segmentation is a potential solution but not discussed in this work, while LLMs can further include the segmentation methods that use vision-language architectures. Besides, cross-domain evaluation, *e.g.*, transferring from a synthetic to a real wide-FoV scene, or from a narrow-FoV camera to a wide-FoV camera, will be further explored in our future work.

References

- [1] I Armeni. Joint 2d-3d semantic data for indoor scene understanding. *arXiv preprint arXiv:1702.01105*, 2017. 1, 2, 5
- [2] Vijay Badrinarayanan, Alex Kendall, and Roberto Cipolla. Segnet: A deep convolutional encoder-decoder architecture for image segmentation. *IEEE transactions on pattern analysis and machine intelligence*, 39(12):2481–2495, 2017. 1, 2
- [3] Angel Chang, Angela Dai, Thomas Funkhouser, Maciej Halber, Matthias Niessner, Manolis Savva, Shuran Song, Andy Zeng, and Yinda Zhang. Matterport3d: Learning from rgb-d data in indoor environments. *arXiv preprint arXiv:1709.06158*, 2017. 1, 2, 5
- [4] Keyan Chen, Bowen Chen, Chenyang Liu, Wenyan Li, Zhengxia Zou, and Zhenwei Shi. Rsmamba: Remote sensing image classification with state space model. *IEEE Geoscience and Remote Sensing Letters*, 2024. 3, 4
- [5] Liang-Chieh Chen, Yukun Zhu, George Papandreou, Florian Schroff, and Hartwig Adam. Encoder-decoder with atrous separable convolution for semantic image segmentation. In *ECCV*, pages 801–818, 2018. 2
- [6] Shoufa Chen, Enze Xie, Chongjian Ge, Runjian Chen, Ding Liang, and Ping Luo. Cyclemlp: A mlp-like architecture for dense prediction. *arXiv preprint arXiv:2107.10224*, 2021. 2
- [7] Xiaokang Chen, Yuhui Yuan, Gang Zeng, and Jingdong Wang. Semi-supervised semantic segmentation with cross pseudo supervision. In *CVPR*, pages 2613–2622, 2021. 6, 7
- [8] Zhao Chen, Vijay Badrinarayanan, Chen-Yu Lee, and Andrew Rabinovich. Gradnorm: Gradient normalization for adaptive loss balancing in deep multitask networks. In *International conference on machine learning*, pages 794–803. PMLR, 2018. 7
- [9] Bowen Cheng, Alex Schwing, and Alexander Kirillov. Per-pixel classification is not all you need for semantic segmentation. *NeurIPS*, 34:17864–17875, 2021. 2
- [10] Jifeng Dai, Haozhi Qi, Yuwen Xiong, Yi Li, Guodong Zhang, Han Hu, and Yichen Wei. Deformable convolutional networks. In *ICCV*, pages 764–773, 2017. 5
- [11] Liuyuan Deng, Ming Yang, Hao Li, Tianyi Li, Bing Hu, and Chunxiang Wang. Restricted deformable convolution-based road scene semantic segmentation using surround view cameras. *IEEE Transactions on Intelligent Transportation Systems*, 21(10):4350–4362, 2019. 3
- [12] Alexey Dosovitskiy. An image is worth 16x16 words: Transformers for image recognition at scale. *arXiv preprint arXiv:2010.11929*, 2020. 3, 4
- [13] Alexey Dosovitskiy, German Ros, Felipe Codevilla, Antonio Lopez, and Vladlen Koltun. Carla: An open urban driving simulator. In *Conference on robot learning*, pages 1–16. PMLR, 2017. 5
- [14] Marc Eder, Mykhailo Shvets, John Lim, and Jan-Michael Frahm. Tangent images for mitigating spherical distortion. In *CVPR*, pages 12426–12434, 2020. 6
- [15] Jun Fu, Jing Liu, Haijie Tian, Yong Li, Yongjun Bao, Zhiwei Fang, and Hanqing Lu. Dual attention network for scene segmentation. In *CVPR*, pages 3146–3154, 2019. 2
- [16] Albert Gu and Tri Dao. Mamba: Linear-time sequence modeling with selective state spaces. *arXiv preprint arXiv:2312.00752*, 2023. 2, 3, 4
- [17] Albert Gu, Tri Dao, Stefano Ermon, Atri Rudra, and Christopher Ré. Hippo: Recurrent memory with optimal polynomial projections. *NeurIPS*, 33:1474–1487, 2020. 4
- [18] Albert Gu, Karan Goel, and Christopher Ré. Efficiently modeling long sequences with structured state spaces. *arXiv preprint arXiv:2111.00396*, 2021. 3
- [19] Jiaqi Gu, Hyoukjun Kwon, Dilin Wang, Wei Ye, Meng Li, Yu-Hsin Chen, Liangzhen Lai, Vikas Chandra, and David Z Pan. Multi-scale high-resolution vision transformer for semantic segmentation. In *CVPR*, pages 12094–12103, 2022. 2
- [20] Michelle Guo, Albert Haque, De-An Huang, Serena Yeung, and Li Fei-Fei. Dynamic task prioritization for multitask learning. In *ECCV*, pages 270–287, 2018. 7
- [21] Meng-Hao Guo, Cheng-Ze Lu, Qibin Hou, Zhengning Liu, Ming-Ming Cheng, and Shi-Min Hu. Segnext: Rethinking convolutional attention design for semantic segmentation. *NeurIPS*, 35:1140–1156, 2022. 1, 2, 6, 7
- [22] Suresh Guttikonda and Jason Rambach. Single frame semantic segmentation using multi-modal spherical images. In *Proceedings of the IEEE/CVF Winter Conference on Applications of Computer Vision*, pages 3222–3231, 2024. 5
- [23] Kaiming He, Xiangyu Zhang, Shaoqing Ren, and Jian Sun. Deep residual learning for image recognition. In *CVPR*, pages 770–778, 2016. 7, 8
- [24] Vincent Tao Hu, Stefan Andreas Baumann, Ming Gui, Olga Grebenkova, Pingchuan Ma, Johannes Fischer, and Bjorn Ommer. Zigma: Zigzag mamba diffusion model. *arXiv preprint arXiv:2403.13802*, 2024. 3
- [25] Tao Huang, Xiaohuan Pei, Shan You, Fei Wang, Chen Qian, and Chang Xu. Localmamba: Visual state space model with windowed selective scan. *arXiv preprint arXiv:2403.09338*, 2024. 3
- [26] Zilong Huang, Xinggang Wang, Lichao Huang, Chang Huang, Yunchao Wei, and Wenyu Liu. Ccnet: Criss-cross attention for semantic segmentation. In *ICCV*, pages 603–612, 2019. 2
- [27] Alexander Jaus, Kailun Yang, and Rainer Stiefelhagen. Panoramic panoptic segmentation: Towards complete surrounding understanding via unsupervised contrastive learning. In *2021 IEEE Intelligent Vehicles Symposium (IV)*, pages 1421–1427. IEEE, 2021. 3
- [28] Juho Kannala and Sami S Brandt. A generic camera model and calibration method for conventional, wide-angle, and fish-eye lenses. *IEEE transactions on pattern analysis and machine intelligence*, 28(8):1335–1340, 2006. 3
- [29] Alex Kendall, Yarin Gal, and Roberto Cipolla. Multi-task learning using uncertainty to weigh losses for scene geometry and semantics. In *CVPR*, pages 7482–7491, 2018. 7
- [30] Alex Krizhevsky, Ilya Sutskever, and Geoffrey E Hinton. Imagenet classification with deep convolutional neural networks. *NeurIPS*, 25, 2012. 3
- [31] Varun Ravi Kumar, Senthil Yogamani, Hazem Rashed, Ganesh Sitsu, Christian Witt, Isabelle Leang, Stefan Milz,

- and Patrick Mäder. Omnidet: Surround view cameras based multi-task visual perception network for autonomous driving. *IEEE Robotics and Automation Letters*, 6(2):2830–2837, 2021. [2](#), [3](#), [6](#), [7](#)
- [32] Kunchang Li, Xinhao Li, Yi Wang, Yinan He, Yali Wang, Limin Wang, and Yu Qiao. Videomamba: State space model for efficient video understanding. *arXiv preprint arXiv:2403.06977*, 2024. [3](#)
- [33] Xuewei Li, Tao Wu, Zhongang Qi, Gaoang Wang, Ying Shan, and Xi Li. Sgat4pass: spherical geometry-aware transformer for panoramic semantic segmentation. *arXiv preprint arXiv:2306.03403*, 2023. [6](#)
- [34] Zechao Li, Yanpeng Sun, Liyan Zhang, and Jinhui Tang. Ctnet: Context-based tandem network for semantic segmentation. *IEEE Transactions on Pattern Analysis and Machine Intelligence*, 44(12):9904–9917, 2021. [2](#)
- [35] Bee Lim, Sanghyun Son, Heewon Kim, Seungjun Nah, and Kyoung Mu Lee. Enhanced deep residual networks for single image super-resolution. In *CVPR workshops*, pages 136–144, 2017. [4](#)
- [36] Yazhou Liu, Yuliang Chen, Pongsak Lasang, and Qunsen Sun. Covariance attention for semantic segmentation. *IEEE Transactions on Pattern Analysis and Machine Intelligence*, 44(4):1805–1818, 2020. [2](#)
- [37] Yue Liu, Yunjie Tian, Yuzhong Zhao, Hongtian Yu, Lingxi Xie, Yaowei Wang, Qixiang Ye, and Yunfan Liu. Vmamba: Visual state space model. *arXiv preprint arXiv:2401.10166*, 2024. [2](#), [3](#), [4](#), [6](#), [7](#), [8](#)
- [38] Ze Liu, Yutong Lin, Yue Cao, Han Hu, Yixuan Wei, Zheng Zhang, Stephen Lin, and Baining Guo. Swin transformer: Hierarchical vision transformer using shifted windows. In *ICCV*, pages 10012–10022, 2021. [7](#), [8](#)
- [39] Jonathan Long, Evan Shelhamer, and Trevor Darrell. Fully convolutional networks for semantic segmentation. In *CVPR*, pages 3431–3440, 2015. [2](#)
- [40] Anam Manzoor, Aryan Singh, Ganesh Sistu, Reenu Mohandas, Eoin Grua, Anthony Scanlan, and Ciarán Eising. Deformable convolution based road scene semantic segmentation of fisheye images in autonomous driving. In *IET Conference Proceedings CP887*, pages 7–14. IET, 2024. [3](#)
- [41] Zhenliang Ni, Xinghao Chen, Yingjie Zhai, Yehui Tang, and Yunhe Wang. Context-guided spatial feature reconstruction for efficient semantic segmentation. *arXiv preprint arXiv:2405.06228*, 2024. [7](#), [8](#)
- [42] Sneha Paul, Zachary Patterson, and Nizar Bouguila. Semantic segmentation using transfer learning on fisheye images. In *2023 International Conference on Machine Learning and Applications (ICMLA)*, pages 445–452. IEEE, 2023. [3](#)
- [43] Sneha Paul, Zachary Patterson, and Nizar Bouguila. Fishsegssl: A semi-supervised semantic segmentation framework for fish-eye images. *Journal of Imaging*, 10(3):71, 2024. [3](#), [6](#), [7](#)
- [44] Xiaohuan Pei, Tao Huang, and Chang Xu. Efficientvmamba: Atrous selective scan for light weight visual mamba. *arXiv preprint arXiv:2403.09977*, 2024. [3](#)
- [45] Clément Ployat, Ola Ahmad, Freddy Lecue, and Farida Cheriet. Adaptable deformable convolutions for semantic segmentation of fisheye images in autonomous driving systems. *arXiv preprint arXiv:2102.10191*, 2021. [3](#)
- [46] Tran Minh Quan, David Grant Colburn Hildebrand, and Won-Ki Jeong. Fusionnet: A deep fully residual convolutional neural network for image segmentation in connectomics. *Frontiers in Computer Science*, 3:613981, 2021. [3](#)
- [47] Olaf Ronneberger, Philipp Fischer, and Thomas Brox. U-net: Convolutional networks for biomedical image segmentation. In *Medical image computing and computer-assisted intervention—MICCAI 2015: 18th international conference, Munich, Germany, October 5–9, 2015, proceedings, part III 18*, pages 234–241. Springer, 2015. [3](#)
- [48] Ahmed Rida Sekkat, Yohan Dupuis, Varun Ravi Kumar, Hazem Rashed, Senthil Yogamani, Pascal Vasseur, and Paul Honeine. Synwoodscape: Synthetic surround-view fisheye camera dataset for autonomous driving. *IEEE Robotics and Automation Letters*, 7(3):8502–8509, 2022. [1](#), [2](#), [5](#)
- [49] Wenzhe Shi, Jose Caballero, Ferenc Huszar, Johannes Totz, Andrew P Aitken, Rob Bishop, Daniel Rueckert, and Zehan Wang. Real-time single image and video super-resolution using an efficient sub-pixel convolutional neural network. In *CVPR*, pages 1874–1883, 2016. [4](#)
- [50] Robin Strudel, Ricardo Garcia, Ivan Laptev, and Cordelia Schmid. Segmenter: Transformer for semantic segmentation. In *ICCV*, pages 7262–7272, 2021. [2](#)
- [51] Cheng Sun, Min Sun, and Hwann-Tzong Chen. Hohonet: 360 indoor holistic understanding with latent horizontal features. In *CVPR*, pages 2573–2582, 2021. [6](#)
- [52] Antti Tarvainen and Harri Valpola. Mean teachers are better role models: Weight-averaged consistency targets improve semi-supervised deep learning results. *NeurIPS*, 30, 2017. [2](#), [6](#), [7](#)
- [53] Zhifeng Teng, Jiaming Zhang, Kailun Yang, Kunyu Peng, Hao Shi, Simon Reiß, Ke Cao, and Rainer Stiefelwagen. 360bev: Panoramic semantic mapping for indoor bird’s-eye view. In *Proceedings of the IEEE/CVF Winter Conference on Applications of Computer Vision*, pages 373–382, 2024. [5](#), [6](#)
- [54] A Vaswani. Attention is all you need. *NeurIPS*, 2017. [3](#), [4](#)
- [55] Wenhai Wang, Enze Xie, Xiang Li, Deng-Ping Fan, Kaitao Song, Ding Liang, Tong Lu, Ping Luo, and Ling Shao. Pvt v2: Improved baselines with pyramid vision transformer. *Computational Visual Media*, 8(3):415–424, 2022. [7](#)
- [56] Wenhai Wang, Jifeng Dai, Zhe Chen, Zhenhang Huang, Zhiqi Li, Xizhou Zhu, Xiaowei Hu, Tong Lu, Lewei Lu, Hongsheng Li, et al. Internimage: Exploring large-scale vision foundation models with deformable convolutions. In *CVPR*, pages 14408–14419, 2023. [5](#)
- [57] Tete Xiao, Yingcheng Liu, Bolei Zhou, Yuning Jiang, and Jian Sun. Unified perceptual parsing for scene understanding. In *ECCV*, pages 418–434, 2018. [6](#), [7](#), [8](#)
- [58] Enze Xie, Wenhai Wang, Zhiding Yu, Anima Anandkumar, Jose M Alvarez, and Ping Luo. Segformer: Simple and efficient design for semantic segmentation with transformers. *NeurIPS*, 34:12077–12090, 2021. [1](#), [2](#), [6](#), [7](#)
- [59] Yuwen Xiong, Zhiqi Li, Yuntao Chen, Feng Wang, Xizhou Zhu, Jiapeng Luo, Wenhai Wang, Tong Lu, Hongsheng Li,

- Yu Qiao, et al. Efficient deformable convnets: Rethinking dynamic and sparse operator for vision applications. In *CVPR*, pages 5652–5661, 2024. 5
- [60] Jing Xu, Wentao Shi, Pan Gao, Zhengwei Wang, and Qizhu Li. Uperformer: A multi-scale transformer-based decoder for semantic segmentation. *arXiv preprint arXiv:2211.13928*, 2022. 4, 7, 8
- [61] Kailun Yang, Xinxin Hu, Luis M Bergasa, Eduardo Romera, Xiao Huang, Dongming Sun, and Kaiwei Wang. Can we pass beyond the field of view? panoramic annular semantic segmentation for real-world surrounding perception. In *2019 IEEE Intelligent Vehicles Symposium (IV)*, pages 446–453. IEEE, 2019. 3
- [62] Kailun Yang, Xinxin Hu, Luis M Bergasa, Eduardo Romera, and Kaiwei Wang. Pass: Panoramic annular semantic segmentation. *IEEE Transactions on Intelligent Transportation Systems*, 21(10):4171–4185, 2019. 3
- [63] Yijun Yang, Zhaohu Xing, and Lei Zhu. Vivim: a video vision mamba for medical video object segmentation. *arXiv preprint arXiv:2401.14168*, 2024. 3, 4
- [64] Senthil Yogamani, Ciarán Hughes, Jonathan Horgan, Ganesh Sistu, Padraig Varley, Derek O’Dea, Michal Uricár, Stefan Milz, Martin Simon, Karl Amende, et al. Woodscape: A multi-task, multi-camera fisheye dataset for autonomous driving. In *ICCV*, pages 9308–9318, 2019. 1, 2, 5, 6
- [65] Yuhui Yuan, Lang Huang, Jianyuan Guo, Chao Zhang, Xilin Chen, and Jingdong Wang. Ocnet: Object context for semantic segmentation. *International Journal of Computer Vision*, 129(8):2375–2398, 2021. 2
- [66] Jiaming Zhang, Kailun Yang, Chaoxiang Ma, Simon Reiß, Kunyu Peng, and Rainer Stiefelwagen. Bending reality: Distortion-aware transformers for adapting to panoramic semantic segmentation. In *CVPR*, pages 16917–16927, 2022. 1, 2, 3, 6, 7
- [67] Jiaming Zhang, Kailun Yang, Hao Shi, Simon Reiß, Kunyu Peng, Chaoxiang Ma, Haodong Fu, Philip HS Torr, Kaiwei Wang, and Rainer Stiefelwagen. Behind every domain there is a shift: Adapting distortion-aware vision transformers for panoramic semantic segmentation. *IEEE Transactions on Pattern Analysis and Machine Intelligence*, 2024. 1, 2, 3, 5, 6, 7
- [68] Yulun Zhang, Kunpeng Li, Kai Li, Lichen Wang, Bineng Zhong, and Yun Fu. Image super-resolution using very deep residual channel attention networks. In *ECCV*, pages 286–301, 2018. 4
- [69] Zeyu Zhang, Akide Liu, Ian Reid, Richard Hartley, Bohan Zhuang, and Hao Tang. Motion mamba: Efficient and long sequence motion generation. In *European Conference on Computer Vision*, pages 265–282. Springer, 2025. 3
- [70] Junwei Zheng, Jiaming Zhang, Kailun Yang, Kunyu Peng, and Rainer Stiefelwagen. Materobot: Material recognition in wearable robotics for people with visual impairments. In *2024 IEEE International Conference on Robotics and Automation (ICRA)*, pages 2303–2309. IEEE, 2024. 1, 2
- [71] Junwei Zheng, Ruiping Liu, Yufan Chen, Kunyu Peng, Chengzhi Wu, Kailun Yang, Jiaming Zhang, and Rainer Stiefelwagen. Open panoramic segmentation. In *European Conference on Computer Vision*, pages 164–182. Springer, 2025. 3
- [72] Sixiao Zheng, Jiachen Lu, Hengshuang Zhao, Xiatian Zhu, Zekun Luo, Yabiao Wang, Yanwei Fu, Jianfeng Feng, Tao Xiang, Philip HS Torr, et al. Rethinking semantic segmentation from a sequence-to-sequence perspective with transformers. In *CVPR*, pages 6881–6890, 2021. 2
- [73] Xu Zheng, Pengyuan Zhou, Athanasios V Vasilakos, and Lin Wang. Semantics distortion and style matter: Towards source-free uda for panoramic segmentation. In *CVPR*, pages 27885–27895, 2024. 6, 7
- [74] Zishuo Zheng, Chunyu Lin, Lang Nie, Kang Liao, Zhijie Shen, and Yao Zhao. Complementary bi-directional feature compression for indoor 360deg semantic segmentation with self-distillation. In *Proceedings of the IEEE/CVF Winter Conference on Applications of Computer Vision*, pages 4501–4510, 2023. 6
- [75] Lianghui Zhu, Bencheng Liao, Qian Zhang, Xinlong Wang, Wenyu Liu, and Xinggang Wang. Vision mamba: Efficient visual representation learning with bidirectional state space model. *arXiv preprint arXiv:2401.09417*, 2024. 3, 4
- [76] Qinfeng Zhu, Yuanzhi Cai, Yuan Fang, Yihan Yang, Cheng Chen, Lei Fan, and Anh Nguyen. Samba: Semantic segmentation of remotely sensed images with state space model. *Heliyon*, 10(19), 2024. 4
- [77] Xizhou Zhu, Han Hu, Stephen Lin, and Jifeng Dai. Deformable convnets v2: More deformable, better results. In *CVPR*, pages 9308–9316, 2019. 2, 5